

Chapter 8

Temperature Dependence of the Nodal Fermi Velocity in Bi2212

8.1 Introduction

The electronic properties of a solid depend heavily on the electronic structure near the Fermi surface, simply because it is these electrons which are most free to move about the solid. Conductivity in the high T_c cuprates displays a highly unusual linear temperature dependence over a wide range of temperatures, which is considered to be a key feature of the cuprates. Electrical current is carried by the electrons right near the Fermi surface, so to lowest order, the conductivity should be proportional to the velocity of those electrons, which is directly measurable in ARPES as it is simply the slope of the dispersion at the Fermi energy. However, the energy and momentum resolution of ARPES has made detailed structure very close to the E_F difficult to measure. This is because in most ARPES experiments the energy broadening $\Delta E > 4.4k_B T$ at the lowest temperatures, in which case the measured MDC dispersion and scattering rate very close to the Fermi energy will no longer reflect the self-energy of the electron system. This can be seen nicely in a simulation by Ingle *et al.* (Ingle et al., 2005), some results of which are shown in figure 8.1. In this figure, the top panel is the simulated spectral function (cutoff by a Fermi function) for an ideal Fermi liquid system. The bottom panel shows the same spectral function convolved with an experimental energy resolution of

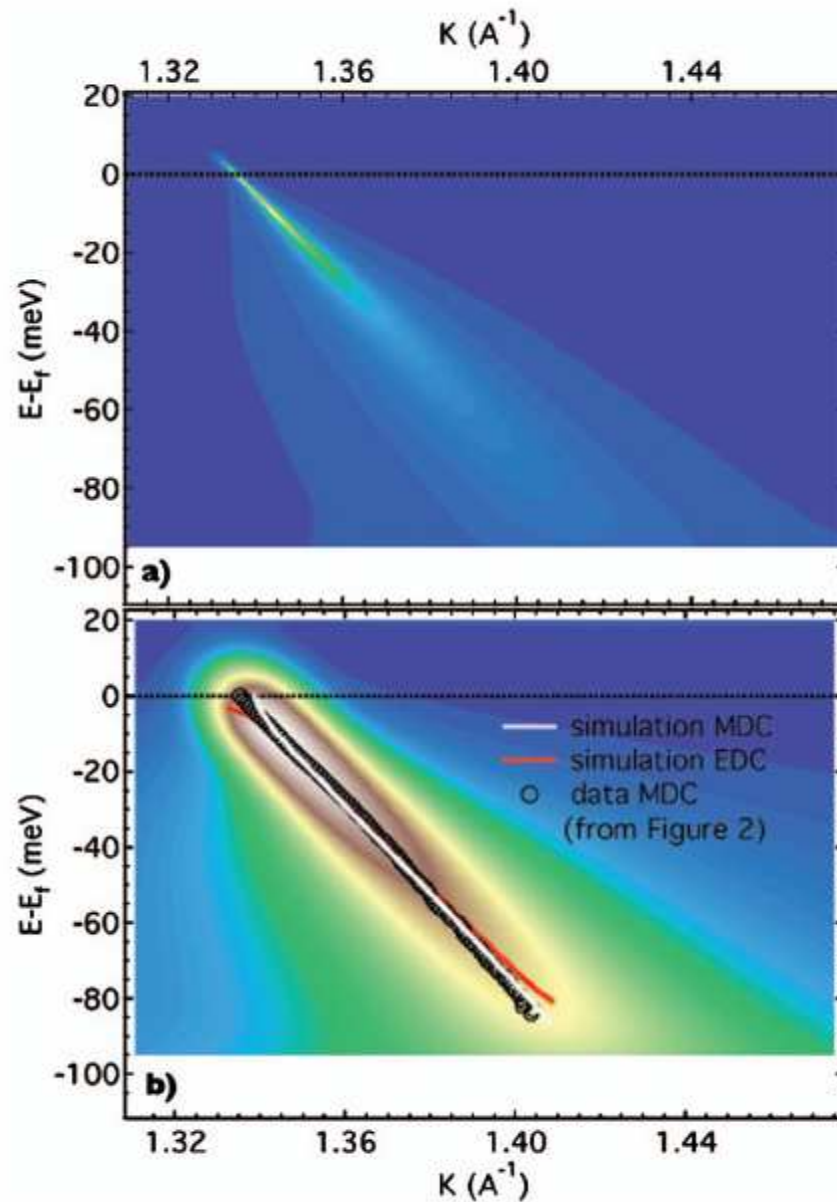


Figure 8.1: (color) Simulation of resolution effects in ARPES. Panel (a) is the spectral function from an ideal Fermi liquid system. Panel (b) is the same spectral function convolved an experimental energy resolution of $\Delta E = 13$ meV and momentum resolution of $\Delta \mathbf{k} = 0.0126 \text{ \AA}^{-1}$ appropriate for synchrotron based ARPES. MDC fits (white line) and EDC fits (red line) to the resulting spectrum are also shown on the plot, and both deviate from the real dispersion (top panel) near E_F . The open circles are ARPES data from Sr_2RuO_4 and are not relevant. Figure originally from Ingle *et al.* (Ingle *et al.*, 2005)

$\Delta E = 13$ meV and momentum resolution of $\Delta \mathbf{k} = 0.0126 \text{ \AA}^{-1}$.¹ The convolved spectra are then analyzed using EDC and MDC analysis, just as would be done for real ARPES data. We know from the simulated spectral function of the top panel that the band in fact crosses the Fermi energy without deviating from its roughly linear path. But the Fits to the simulation in the bottom panel diverge close to E_F , with a strong upturn in the MDCs and a downturn in the EDCs. For the laser ARPES experiments, with energy resolution $\Delta E < 11$ meV and $\Delta k = 0.0018 \text{ \AA}^{-1}$, this is not a concern down to temperatures as low as 25 K. Because of this, we were able to resolve the fine details in the near-Fermi dispersion much more accurately than ever before. This chapter discusses the observation of a linear temperature dependence to the nodal Fermi velocity. This effect may be related to the temperature dependence of the dispersion kink, but at this stage the cause of both effects and their connection to each other is unknown.²

8.2 Experimental

The laser ARPES experiments of this section were carried out using the techniques described in section 6.2. Synchrotron data was collected at beamline 12.0.1 at the Advanced Light Source in Berkeley, CA.³ In addition to the optimally doped samples of chapter 6, heavily overdoped Bi2212 samples were measured with laser ARPES. These samples were sealed in VCR cap-plug pairs containing liquid oxygen, which were then heated to 400°C - 500°C. This results in an oxygen pressure of more than 1000 atm, producing very heavily overdoped samples (Mihaly, Kendziora, Hartge, Mandrus, & Forro, 1993; Gromko, 2001). We have not been able to measure the transition temperature of the heavily over-

¹ These values are appropriate for the resolution of the experiments of Ingle *et al* (Ingle et al., 2005).

² This effect was observed simultaneously by us and the Dresden group (Kordyuk et al., 2006), although none of the results have yet been published.

³ The synchrotron data was collected by Fraser Douglas and Zhe Sun.

doped samples used in this study, but we expect it to be in the 60 - 70 K range based on past experience with this annealing technique (Gromko et al., 2003).

8.3 Temperature dependent nodal Fermi velocity in Bi2212

Figure 8.2 shows MDC derived nodal dispersion in optimally doped Bi2212 from laser ARPES at 4 different temperatures. The high energy dispersion in the region below the kink does not change with temperature, but the dispersion near the Fermi energy shows a clear change with temperature. Specifically, the Fermi velocity (the slope of the dispersion at the Fermi surface) can be clearly tracked in this data. We estimate the Fermi velocity with a linear fit to the dispersion about the Fermi energy, the temperature dependence of which is shown in figure 8.3. In addition to the result from the optimal sample of figure 8.2, the Fermi velocity from a heavily overdoped sample is shown, as well as results from a lightly overdoped sample measured using synchrotron photons. The temperature dependence is noticeably stronger in the optimal sample. This trend is qualitatively similar to what is observed in the strength of the dispersion kink (Gromko et al., 2003) which may indicate a connection between the two effects.

The temperature dependence of the Fermi velocity and kink strength has also been observed in optical conductivity data (Hwang et al., 2004; Puchkov, Basov, & Timusk, 1996), an example of which is shown in figure 8.4. Although none of the authors has discussed the temperature dependence of the Fermi velocity explicitly, it can be seen as a change in the $\text{Re}\Sigma^{\text{op}}$ at zero frequency. Since the optical measurements are not \mathbf{k} -resolved, $\text{Re}\Sigma^{\text{op}}$ contains contributions from the entire Fermi surface and is not expected to look identical to $\text{Re}\Sigma$ measure with ARPES.

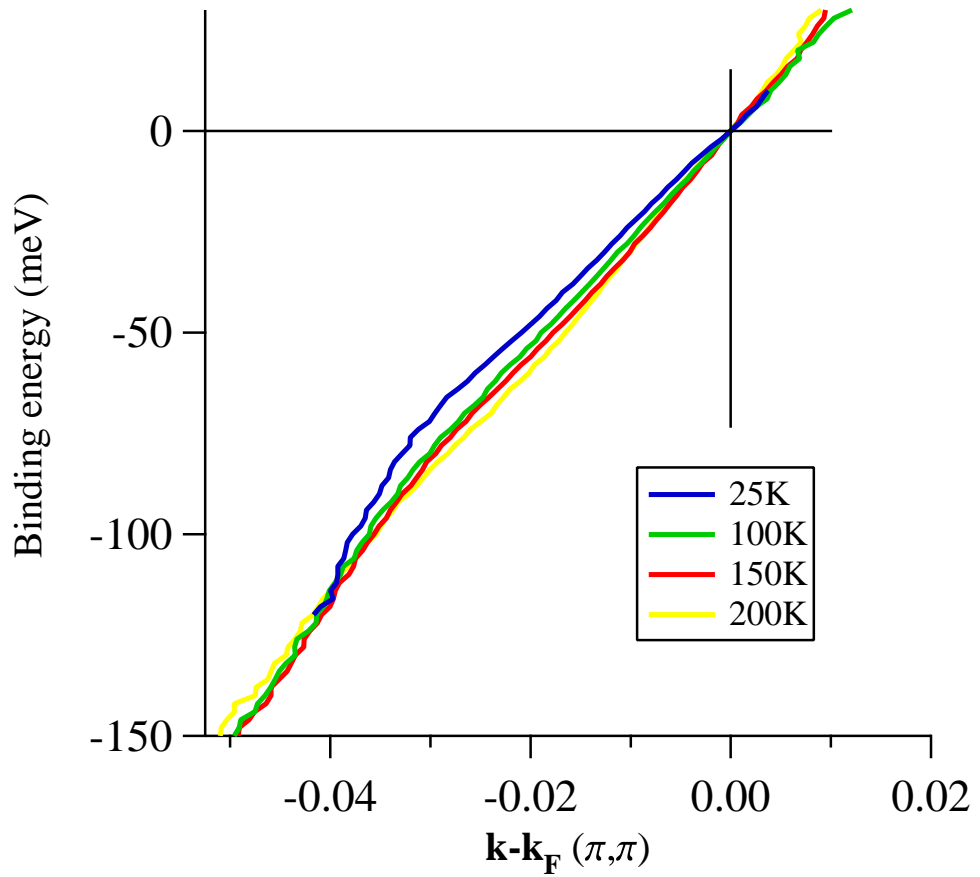


Figure 8.2: (color) Temperature dependence of the nodal dispersion, derived from Lorentzian MDC fits, in optimally doped Bi2212. The kink coupling strengthens with decreasing temperature, leading to a temperature dependent Fermi velocity.

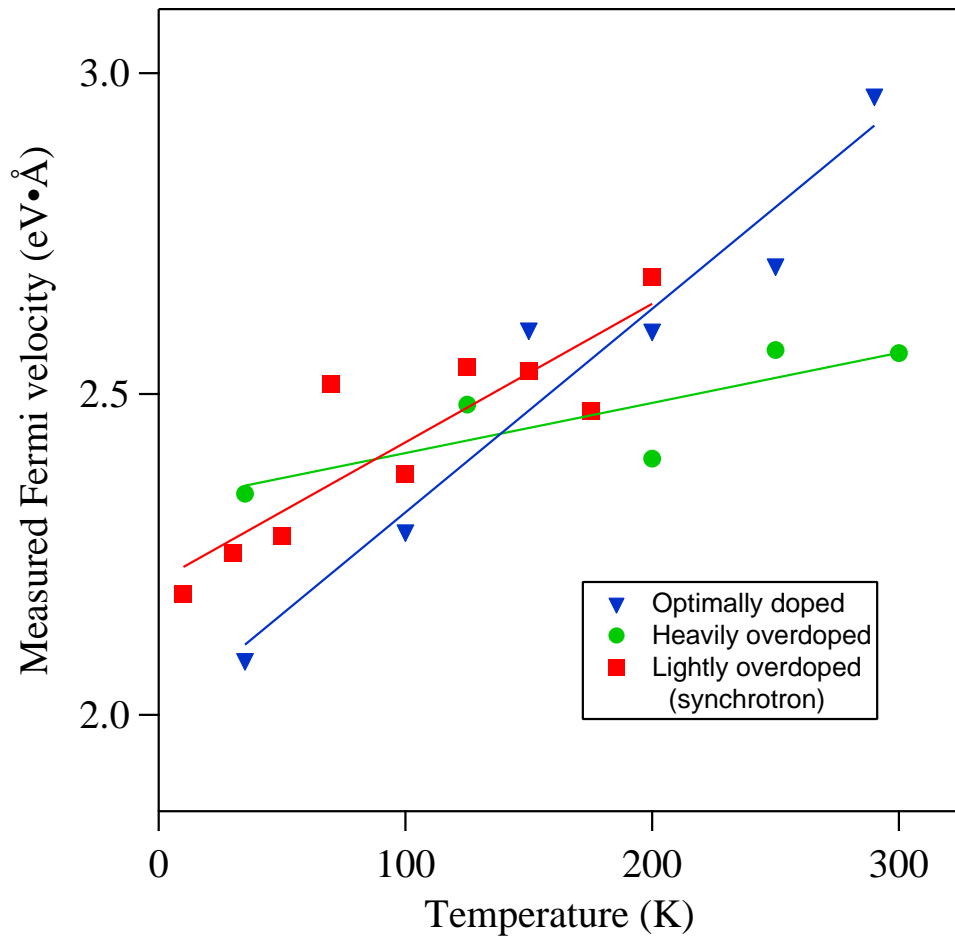


Figure 8.3: (color) Temperature dependence of the Fermi velocity from optimal (blue triangles) and heavily overdoped (green dots) measured with laser ARPES and a lightly overdoped sample measured at beamline 12.0.1 at the ALS. The solid lines are linear fits to the data.

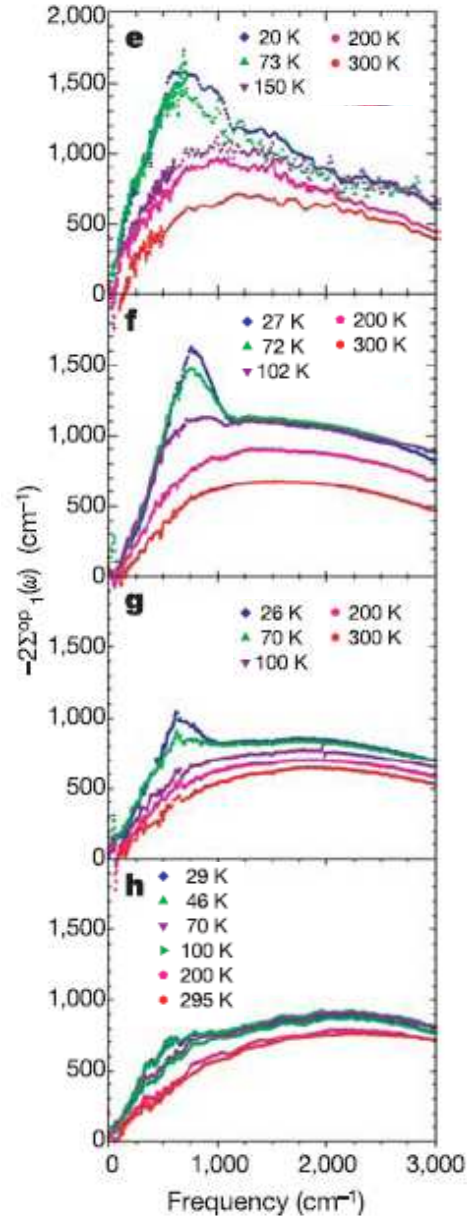


Figure 8.4: (color) Temperature dependence of $\text{Re}\Sigma^{\text{op}}$ in optimally doped Bi2212, measured with Fourier transform infrared spectroscopy (FTIR). The samples are UD67K (e), OP96K (f), OD82K (g), OD60K (h). Σ^{op} is the optical self energy, determined from the optical conductivity through Kramers-Kronig analysis of the reflectivity. Within the extended Drude model, these are related by $\sigma(\omega) = -i\omega_p^2/4\pi[2\Sigma^{\text{op}}(\omega) - \omega]$. The temperature and doping dependence of the kink and $\text{Re}\Sigma^{\text{op}}$ can be seen clearly in the data, and is qualitatively in agreement with the laser ARPES data. Note that the optical measurements are not \mathbf{k} -resolved, and so are not expected to match the nodal ARPES data exactly. Figure from Hwang *et al.* (Hwang *et al.*, 2004)

8.4 Simulations of the electron-boson coupling

In order to try and understand the origin of the observed temperature dependence, we have simulated the effects of different electron boson couplings on the self-energy. The general temperature dependence of the scattering rate $\frac{1}{\tau_{imp}}$ from an arbitrary electron-boson coupling (defined by the boson spectrum $\alpha^2 F$)⁴ has been derived from many-body calculations (Shulga, Dolgov, & Maksimov, 1991; Puchkov et al., 1996),

$$\frac{1}{\tau}(\omega, T) = \frac{\pi}{\omega} \int_0^{\infty} d\Omega \alpha^2 F(\Omega) \left[\begin{array}{l} 2\omega \coth\left(\frac{\Omega}{2T}\right) - (\omega + \Omega) \coth\left(\frac{\omega + \Omega}{2T}\right) \\ + (\omega - \Omega) \coth\left(\frac{\omega - \Omega}{2T}\right) \end{array} \right] + \frac{1}{\tau_{imp}} \quad (8.1)$$

where $\frac{1}{\tau_{imp}}$ is the impurity scattering rate. We begin with the simplest possible boson spectrum, an Einstein phonon for which $\alpha^2 F = E_0 \delta(E - E_0)$. In this case the integral of equation 8.1 can be done trivially. The mass enhancement $\lambda(\omega)$ can then be calculated via Kramers-Kronig transformation.

$$\lambda(\omega) = \frac{2}{\pi} \int_0^{\infty} \frac{1/\tau(\omega)}{\Omega^2 - \omega^2} d\Omega \quad (8.2)$$

These integrals were performed numerically using MathCad (Mathsoft). Figure 8.5 shows the calculated $\frac{1}{\tau}$ and λ from this simulation as a function of energy and temperature, as well as the resulting Fermi velocity. The simulated temperature dependence of the Fermi velocity does not match the data: it not only displays non-linear behavior for the case of $\alpha^2 F = E_0 \delta(E - E_0)$, but it is non-monotonic. However, the temperature dependence of the dispersion kink from this simulation does recreate the behavior that is observed in the data. The dispersion smoothly evolves as temperature decreases, forming a sharp kink at low

⁴ This notation specifically refers to the Eliashberg function specific to phonons, however, equation 8.1 is thought to hold for any bosonic spectrum (Dolgov & Shulga, 1995)

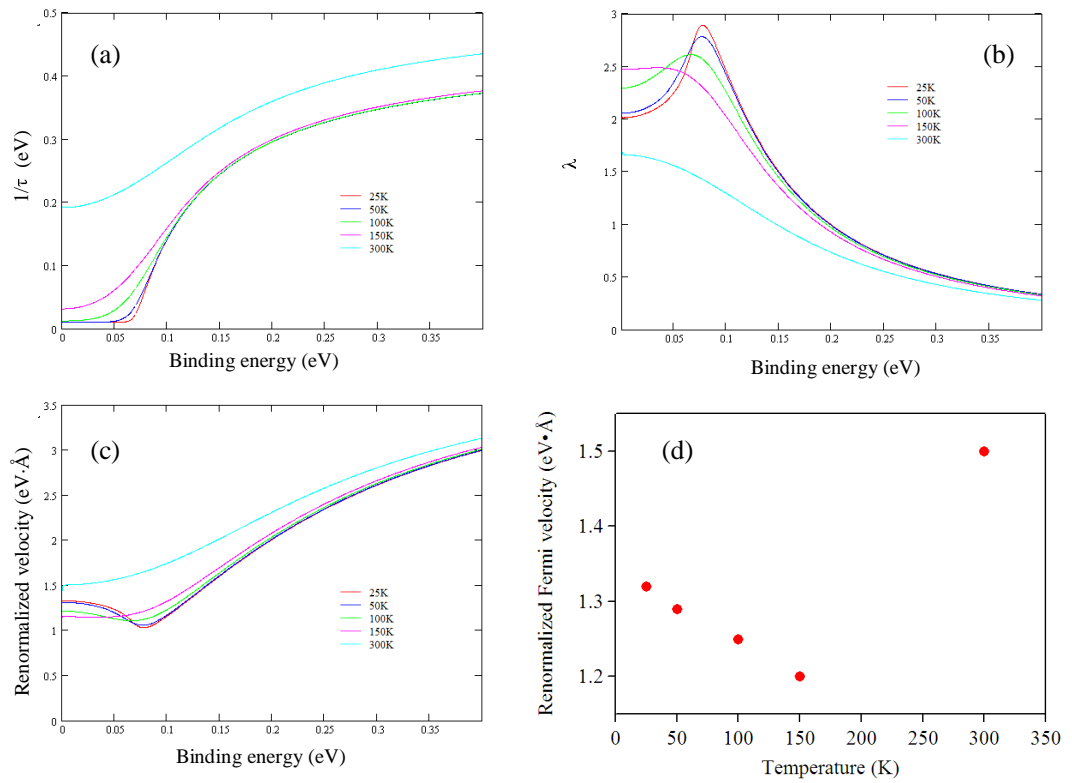


Figure 8.5: (color) Simulation of the electronic coupling to an Einstein phonon at 70 meV from equation 8.1 using $\alpha^2 F = E_0 \delta(E - E_0)$. The scattering rate $\text{Im}\Sigma$ (a), mass renormalization λ (b) and renormalized velocity (c) are shown as a function of binding energy over the experimental range of temperatures. Panel (d) is the predicted temperature dependence of the Fermi velocity v_F , which is non-linear and non-monotonic.

temperature. This can be seen in both the mass enhancement λ and the renormalized velocity. Similar results were obtained from a square spectrum (5-10 meV wide), though the changes in $\frac{1}{v}$ and λ were slightly less localized about the mode energy E_0 . But even a 10 meV wide square spectrum produced results similar to the δ -function case, resulting in a Fermi velocity that is non-monotonic in temperature.

The same procedure was carried out for the case of electrons coupling to spin-fluctuations, where

$$\alpha^2 F = \frac{E/E_0}{1 + (E/E_0)^2} \quad (8.3)$$

is thought to be the appropriate boson spectrum (Millis, Monien, & Pines, 1990). This spectrum is qualitatively different from the Einstein phonon case of figure 8.5 in that it extends over a wide energy range without a sharp cut off (figure 8.6). The results of the spin fluctuation simulation are shown in figure 8.7 and are dis-

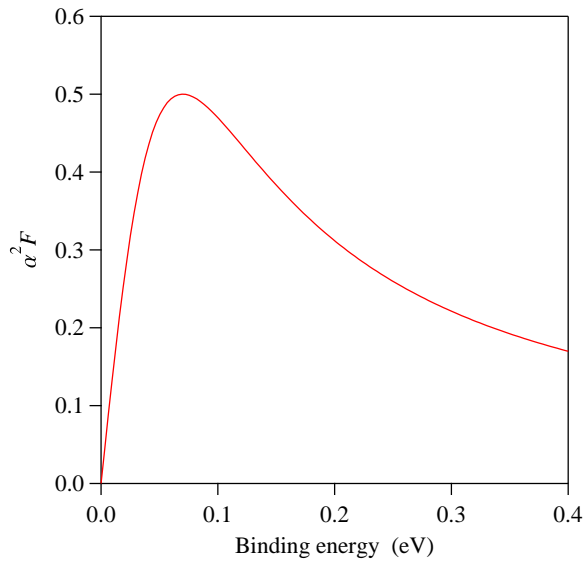


Figure 8.6: (color) The spectrum $\alpha^2 F$ for the coupling of electrons to spin fluctuations (Millis et al., 1990) (equation 8.3).

tinctly different from the Einstein phonon case. In the spin fluctuation simulation, a linear temperature dependence of the Fermi velocity is produced which matches

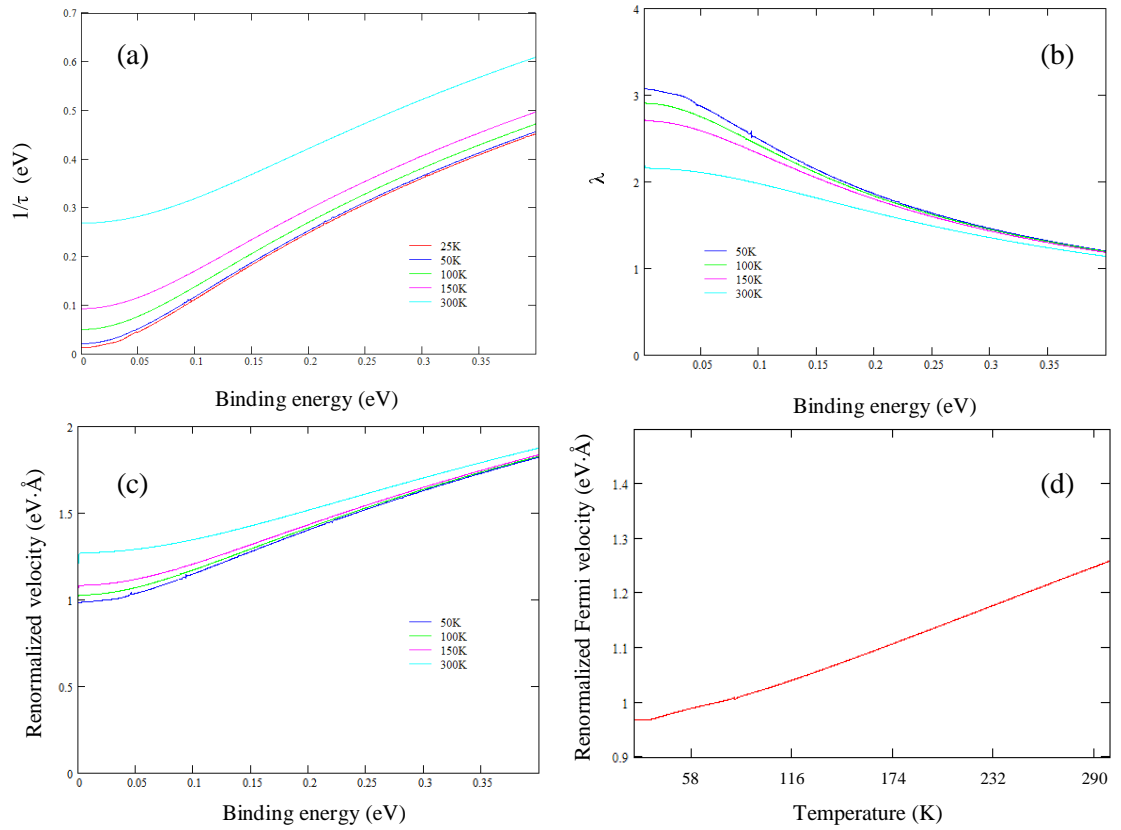


Figure 8.7: (color) Simulation of coupling to spin fluctuations, equation 8.1 with $\alpha^2 F(E) = \frac{E/E_0}{1+(E/E_0)^2}$. Shown are the scattering rate (a) and the mass enhancement (b) and the renormalized velocity (c) as a function of energy. Also shown is the temperature dependence of the Fermi velocity (d), which is roughly linear in agreement with the data.

the data qualitatively very well.⁵ However, there is no longer a sharp kink in the dispersion as is present in both the data and the Einstein phonon simulation.

These simulations suggest two qualities in the electron-boson coupling required to produce the observed temperature dependence of the kink and Fermi velocity. First, the bosonic coupling spectrum $\alpha^2 F$ must extend over a broad energy range in order to produce a linear temperature dependence to the Fermi velocity. Second, $\alpha^2 F$ must have contain a sharp spike in order to produce the observed dispersion kink and it's temperature dependence. It certainly possible that such effects could arise from the coexistence of electronic coupling to phonons and spin fluctuations.

8.5 Summary

A linear temperature dependence of the nodal Fermi velocity was observed in Bi2212 with laser ARPES. The temperature effects on the nodal self energy of several different bosonic couplings were simulated. Although it is still to early to say what is the cause of the observed effects, it is clear from these simulations that the bosonic spectrum must extend over a broad energy range in order to result in the observed temperature dependence of the Fermi velocity, but must also contain a sharp peak in order to produce the dispersion kink.

The ability to study the self-energy close to the Fermi energy at low temperature was made possible by the resolution improvements of laser ARPES. These improvements may also make possible an alternative rout to determination of the electron-boson coupling spectrum $\alpha^2 F$. In the limit of very low temperature, equation 8.1 reduces to the well known expression derived by Allen (Allen, 1971),

$$\frac{1}{\tau}(\omega, T \rightarrow 0) = \frac{2\pi}{\omega} \int_0^{\omega} d\Omega (\omega - \Omega) \alpha^2 F(\Omega) + \frac{1}{\tau_{imp}} \quad (8.4)$$

⁵ The overall scaling of the velocity in figure 8.7 d is controlled by the bare velocity.

Recall that $\frac{1}{\tau}$ can directly be measured with ARPES, it is simply the half-width of the MDCs. Therefore if we differentiate this expression, then boson spectrum $\alpha^2 F$ can be directly related to the MDC width ($\frac{1}{\tau}$).

$$\frac{d}{d\omega} \left[\frac{1}{\tau} \right] \propto \alpha^2 F(\omega) \quad (8.5)$$

As of right now, resolution and temperature have not reached the level where this procedure is completely reliable. However, with improvements to our system currently underway, this will be possible very soon.